Journal of Molecular Liquids 405 (2024) 125069

Contents lists available at ScienceDirect

Journal of Molecular Liquids

journal homepage: www.elsevier.com/locate/molliq

Characterization of camphor: thymol or dl-menthol eutectic mixtures; Structure, thermophysical properties, and lidocaine solubility

Nuria Padilla [a], Ignacio Delso [b], Fernando Bergua [a,c], Carlos Lafuente [a,c], Manuela Artal [a,c,*]

[a] Departamento de Química Física, Facultad de Ciencias, Universidad de Zaragoza, Zaragoza, Spain
[b] School of Pharmacy, University of East Anglia, Norwich, United Kingdom
[c] Instituto Agroalimentario de Aragón - IA2 (Universidad de Zaragoza - CITA), Zaragoza, Spain

ARTICLE INFO

Keywords:
Camphor
Thymol
Menthol
Eutectic solvents
Thermophysical properties
Lidocaine solubility

ABSTRACT

The low solubility of drugs in aqueous media is a major problem for the pharmaceutical industry. Among the solutions proposed, the use of eutectic mixtures can be highlighted. In them, the components used can also increase the therapeutic advantages of the active principle. In this work, we analyzed the solubility of lidocaine in mixtures of camphor + thymol or dl-menthol. These binary eutectic solvents were also characterized. For all this, several NMR techniques were used and different thermophysical properties (density, speed of sound, refraction index, isobaric molar heat capacity, surface tension, and kinematic viscosity) were measured. The results indicated that the interaction of camphor with thymol was stronger than with dl-menthol, providing a more compact fluid. On the contrary, the steric hindrance was greater in the mixture with dl-menthol, giving rise to a more viscous liquid. Furthermore, the lidocaine was significantly more soluble (up to 540 times) in these mixtures than in water. The lidocaine showed the strongest interactions with thymol molecules, somewhat weaker with dl-menthol, and the weakest were with camphor ones.

1. Introduction

Most drugs on the market or under development are poorly soluble in water, which leads to low bioavailability and permeability [1]. This fact limits its application since it implies supplying large doses, and provokes a delayed onset of action and an erratic absorption process [2]. The use of active principles (APIs) in the form of crystals, salts, emulsions, or mesoporous silica can solve part of the drawbacks [3]. Another alternative raised in the literature is the preparation of eutectic mixtures that can act as good solvents for APIs or that, in themselves, already have therapeutic activity [4–9]. Eutectic solvents can be defined as a mixture of two or more compounds whose eutectic melting temperature (T_f) is lower than that calculated assuming ideal behavior (T_f^{id}) [10]. Both the establishment of a network of hydrogen bonds between the components and the entropic effect that favors mixing contribute to the decrease of the fusion point. They are called deep eutectic solvents (DESs) if the difference $\left(T_f^{id} - T_f\right)$ is a high positive value. The chemical formula Cat^+X^-zY was initially proposed by Smith et al. [11] and four types of DESs were described. Types I, II, and IV correspond to eutectics in which Cat^+X^- are anhydrous or hydrated inorganic halide salts. Type III combines organic salts as hydrogen bond acceptors and metabolites as donors. The four types give rise to hydrophilic mixtures and due to their composition, type III is the most interesting from an environmental point of view and is often called natural DES (NADES). Since 2015, a new type of eutectic mixtures formed by non-ionic compounds are being studied [12–14]. They have been classified as type V and their hydrophobicity stands out among their characteristics. The $\left(T_f^{id} - T_f\right)$ of most of these mixtures is very small, that is, they have a quasi-ideal behavior. In these cases, they are called hydrophobic eutectic solvents (hESs). Among the most used components to prepare hESs, the family of terpenes stands out.

Terpenes are organic compounds derived from isoprene (C_5H_8) and are the skeleton of a wide variety of metabolites. They are classified depending on the number of C_5H_8 unities. Thus, monoterpenes consist of 2 units and can be linear, monocyclic, and bicyclic. The replacement of methyl groups by functional groups, generally containing oxygen, gives rise to the corresponding terpenoids. The monoterpenoids used herein were camphor (C), thymol (T), and dl-menthol (M). Camphor (1,7,7-trimethylbicyclo[2,2,1]heptan-2-one) has a bicyclic structure. From nature natural sources, the dextrorotatory form is obtained by the

* Corresponding author at Departamento de Química Física, Facultad de Ciencias, Universidad de Zaragoza, Zaragoza, Spain.
E-mail address: martal@unizar.es (M. Artal).

https://doi.org/10.1016/j.molliq.2024.125069
Received 10 January 2024; Received in revised form 17 April 2024; Accepted 18 May 2024
Available online 19 May 2024

distillation of laurel tree wood. The laevorotatory form is only provided by chemical synthesis. The bicyclic hydrophobic region is responsible for the biological properties as insecticide, antiviral, anticancer, or analgesic [15]. Camphor and derivates have been widely used in traditional medicine and the cosmetic industry because it is a penetration enhancer from transdermal [16]. The heat effect produced by this terpenoid upon contact with the skin is well known. It is an activator of several transient receptors' potential channels, improving blood flow after its application [17]. All of this, and its low price make C one of the most commercial chemicals. About its toxicity, C is considered a toxic compound and the lethal dose in adults is within 50–500 mg/kg [18]. Despite this, several international agencies such as OTC (Over-the-Counter) and the FDA (Food and Drug Administration) have established the value of 11 % as the maximum amount of C in the products [19] so poisoning is rare. Thymol (5-Methyl-2-(propan-2-yl)phenol) and dl-menthol (5-Methyl-2-(propan-2-yl)cyclohexan-1-ol) contain an alcohol group. From a structural point of view, the only difference between them is the presence of an aromatic ring in the first one versus a cyclic one in the second one. This fact provokes great differences in their properties. In nature, they are extracted from thyme and mint, respectively and both have been classified by the U.S Food & Drug Administration (FDA) as food additives Generally Recognized As Safe (GRAS) with low toxicity levels [20]. They have an aroma and flavour characteristic so have widely used in the food and cosmetic industries. In addition, they exhibit biological activity against inflammatory, microbial, or oxidative processes among others, they are common additives in pharmacologic formulations, increasing the permeation capacity [21,22]. The M is capable of stimulating the TRPM8 thermoregulatory receptor, causing a cold effect, unlike the ketone terpenoid [23]. In addition to the characteristics of these substances separately, the blends between them have shown good permeation properties. The C: T eutectic mixture has exhibited a synergic effect showing a better antimicrobial response than other pharmaceutical preparations with the pure compounds and an improvement in the solubility of compounds [24,25]. Literature reports the enhancement of skin permeation of drugs as captropril or glabridin or fluconazole using blends of C and M [26–29]. Also, it has been used for microextraction of polar and non-polar acids from urine and in preparing antifungal transdermal spray formulations [30–32]. Finally, this mixture is used as the base of commercial balms that are widely used in sports.

Some authors [26,33–36] have studied the physical properties of mixtures of C and T or M but only data from two papers can be numerically compared with ours. Martins et al. [34] published the phase equilibria and properties as density and viscosity of the equimolar mixtures of C: T or C: M in a wide T range. Abdallah et al. [33] determined several thermophysical properties of the C: T (1:1) mixture at 298 K. No results from Nuclear Overhauser Effect SpectroscopY (NOESY) and Diffusion-Ordered SpectroscopY (DOSY) experiments were found.

The addition of a third active principle as lidocaine (L) to these mixtures would increase their applications. Lidocaine (2-(diethylamino)-*N*-(2,6-dimethyl phenyl)acetamide) is an active principle with amino and amide groups that is mainly used as a local anesthetic by oral, intravenous, and cutaneous routes. Another important use includes the treatment of ventricular tachycardia by blocking the sodium channel [37]. Other APIs as prilocaine or epinephrine are included in the commercial formulations of lidocaine. Considering the properties of the monoterpenoids above reported and the uses of lidocaine, a joint formulation could be of interest.

The aim of this paper is focused on the physicochemical characterization of two hydrophobic eutectic solvents composed of camphor and thymol or dl-menthol. First, several NMR experiments displayed the nature of the interactions between the components of the mixture and allowed us to obtain their diffusion coefficients. Second, six thermophysical properties were measured and others were calculated at several temperatures and at a pressure of 0.1 MPa. Finally, the solubility of lidocaine in these mixtures was determined and discussed using NMR techniques.

2. Materials and methods

2.1. Materials

The compounds used to prepare the hydrophobic mixtures were thymol (T), dl-menthol (M), and camphor (C). For the latter, we have used the 1R(+)(98 %) isomer. Also, lidocaine was used in the solubility study. All of them were provided by Sigma–Aldrich and used as supplied. Their properties and structures are reported in Table 1.

2.2. Preparation of hESs

The composition of the mixtures studied was camphor: thymol (1:1, molar ratio) and camphor:menthol (1:2, molar ratio) and are referred to below as C:T (1:1) and C:M (1:2). Their molar masses were calculated as $M = \sum_i M_i x_i$ and the values were 151.23 and 152.92 g·mol^{-1}, respectively. The same preparation method was used for both mixtures. The components were weighed in the appropriate proportions with a Sartorius PB210S balance ($u(m) = 1{\cdot}10^{-4}$ g). The Erlenmeyer flask was then placed in a silicone bath with stirring and slight heating (323 K) until a homogeneous liquid was formed. The samples were slowly cooled and kept in the dark at 298 K until use. The water content in the mixtures was determined by triplicate by the Karl-Fischer method (automatic titrator Crison KF 1S-2B) and was lower than 300 ppm in all cases.

2.3. Characterization

2.3.1. NMR spectra

The NMR experiments were carried out with a Bruker AVANCE spectrophotometer (400 MHz) thermostated at 300 K. For each ^{1}H NMR spectrum, 8 scans (one-pulse sequence program *zg30*) with a spectral width of 16 ppm, centered at 5 ppm, and with a relaxation time of 3 s were recorded. For each ^{13}C NMR spectrum, 64 scans (APT sequence program *jmod*) with a spectral width of 240 ppm, centered at 110 ppm, and a relaxation time of 2 s were acquired. Several routines such as DQF-COSY, ^{1}H–^{13}C HSQC, and ^{1}H–^{13}C HMBC (Bruker pulse programs cosygpmfqf, hsqcedetgp, and hmbclpndqf, respectively) were used to the signal assignation. In addition, NOESY and DOSY were performed to evaluate the type of interactions between the components of the mixture. The pulse programs were *noesygpph* and *stebpgp1s,* respectively. Eight scans with a spectral width of 16 ppm and centered at 5 ppm were carried out for each experiment. For NOESY experiments a mixing time, *D*8, of 1 s was used. DOSY experiments were recorded with 32 linear gradient increments from 2 to 98 %. Finally, the diffusion coefficients, D, were calculated from the DOSY spectra with the following equation:

$$I(g) = I_0 \exp\left[-D\gamma_H^2 g^2 \delta^2 (\Delta - \delta/3) \right] \quad (1)$$

where $I(g)$ is the resonance intensity measured for a given gradient strength, g; I_0 is the NMR signal in the absence of the gradient pulse; γ_H is the gyromagnetic ratio of the hydrogen nucleus; δ is the duration of the bipolar gradient pulse; and Δ is the diffusion time. At diluted conditions, the solvent used was $CDCl_3$ and the reproducibility of D coefficients was better than 1 %.

2.3.2. Thermophysical properties

The properties measured in the study of the eutectic mixtures were the density (ρ), speed of sound (u), refraction index (n_D), isobaric molar heat capacity ($C_{p,m}$), surface tension (γ), and kinematic viscosity (ν). For that, several devices whose techniques have been widely described in the literature were used and therefore, only a summary table is presented here. Table 2 collects, for each property, the type of apparatus, the standard uncertainty in the temperature ($u(T)$), the calculated combined expanded uncertainties for each property ($U_c(Y)$), and the

Table 1
Chemicals used in this work.

Chemical (Acronym)	CAS No	Purity [a]	M/g·mol^{-1}	T_f/K	Structure
Camphor (C)	464–49-3	>0.98	152.23	451.5 ± 0.01 [b]	
Thymol (T)	89–83-8	>0.985	150.22	322.5 ± 0.5 [c]	
DL-Menthol (M)	89–78-1	>0.99	156.27	Polymorph- α 307.4 ± 0.5 [d] Polymorph- β 300.3 ± 0.5 [d]	
Lidocaine (L)	137–58-6	>0.98	234.34	340.7 [b]	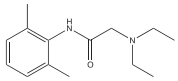

[a] As stated by the supplier (mass fraction); [b] [38]; [c] (Bergua et al., 2021); [d] [40].

Table 2
Summary of the devices used in the thermophysical characterization.

Property	Devices	$u(T)$/K	$U_c(Y)$ [a]	$MRD(Y)$ [b]/%
ρ	Oscillating U-tube density meter, Anton Paar DSA 5000	0.005	0.05 kg·m^{-3}	0.004
u	Sing-around technique in a fixed-path interferometer, Anton Paar DSA 5000	0.005	0.5 m·s^{-1}	0.026
n_D	Standard Abbe refractometer, Abbemat-HP refractometer Dr. Kernchen	0.01	2·10^{-5}	0.007
$C_{p,m}$	Differential scanning calorimeter, TA Instruments DSC Q2000	0.5	1 %	0.028
γ	Drop volume tensiometer, Lauda TVT-2	0.01	1 %	0.21
ν	Capillary viscosimeter Ubbelohde, Schoot-Geräte AVS-440	0.01	1 %	0.28

[a] The combined expanded uncertainty (0.95 level of confidence, k=2); [b] $MRD(Y) = \frac{100}{n}\sum_{i=1}^{n}\left|\frac{Y_{i,lit} - Y_{i,exp}}{Y_{i,exp}}\right|$.

mean relative deviations ($MRD(Y)$) obtained from the test with benzene [41,42].

2.4. Solubility measurements

The procedure to determine the solubility of lidocaine (W_L, in m $g_L/g_{solvent}$) in water or in ESs was the called shake-flask method [43]. The solid solute was added to about 20 ml of solvent in a thermostatted double-walled flask until oversaturation was reached. The heterogeneous system was stirred for 12 h at 298.15 K to ensure the thermodynamic equilibrium. Following this, the sample was sedimented and several aliquots were centrifuged, filtered (PES syringe filter, 0.22 μm), and analyzed. Each experiment was performed in triplicate. The concentration of L in water was measured by UV–VIS spectroscopy with a double-beam spectrum VWR 6300 PC with an accuracy of $u(\lambda) = \pm 0.2$ nm. To quantify the mass fraction of L dissolved in water, a calibration curve of L in ethanol was built by determining the absorbance of several samples at $\lambda = 264$ nm (Abs_{max}). At this wavelength, the spectral peak of L is maximum and is not influenced by ethanol. The equation obtained was:

$$Abs_{max} = 1350.8 \bullet W_L ; R^2 = 0.997 \quad (2)$$

The detection and quantification limits were LD = 3.75·10^{-6} $g_L/g_{solvent}$, and LQ = 1.25·10^{-5} $g_L/g_{solvent}$. On the other hand, the solubility of L in the eutectic mixtures was calculated by the analysis of the NMR spectra because T and C absorb UV–VIS radiation at a similar wavelength as L.

3. Results and discussion

In this section, we present the structure and the physicochemical properties of the C:T (1:1), and C:M (1:2) mixtures. The compositions were chosen close to the eutectic point of each system to ensure a liquid phase over a wide range of temperatures [34].

3.1. Structural study

For the C:T (1:1) mixture, the one-dimensional spectra (Fig. S1) showed that the compounds had not undergone degradation in the mixing process, and allowed us to confirm experimentally that the molar ratio of the mixture was correct. Comparison with the spectra of the individual components showed that only the hydroxy group in T suffered a significant change in chemical shift in the ^{1}H spectrum, due to the establishment of a strong hydrogen bond, as well as the carbon atom directly bound to the OH group in T and the carbonyl in C, when comparing the corresponding ^{13}C spectra. From the NOESY experiment (Fig. 1a), it can be observed that all cross-peaks were positive as opposed to negative diagonal peaks, and they mainly correspond to the expected intramolecular nOe interactions due to proximity (less than 4 Å), for both components. However, a few intermolecular cross-peaks are detected. One peak correlating protons 5 and 6 in T, is too far apart to be intramolecular nOe signal. Less intense cross-peaks are observed among methyl groups (5 and 6 protons) in T and aliphatic protons of C (a and f protons). These results confirm the existence of dispersive and hydrophobic interactions in this system. Nevertheless, the small amount of intermolecular cross-peaks and the opposed sign to the diagonal indicate that a strong supramolecular structure has not been formed and molecules in the system move mainly independently [44]. DOSY experiments were performed to estimate the mobility of several species. Three groups of signals were obtained when studying the neat mixture (Fig. 1b). They corresponded to the aliphatic hydrogens of C, the aliphatic and aromatics hydrogens of T, and the hydroxyl group of T. From them, the diffusion coefficients were calculated with the eq. (1). Also, the mixture was diluted with 90 % $CDCl_3$, and its mobility was determined. All values are listed in Table 3. In the neat sample, the diffusivity of C was lower than that of T, even though camphor exhibited a higher value than thymol when diluted in $CDCl_3$. This fact could be justified by the stoichiometry of the transient intermolecular complexes. One molecule of C

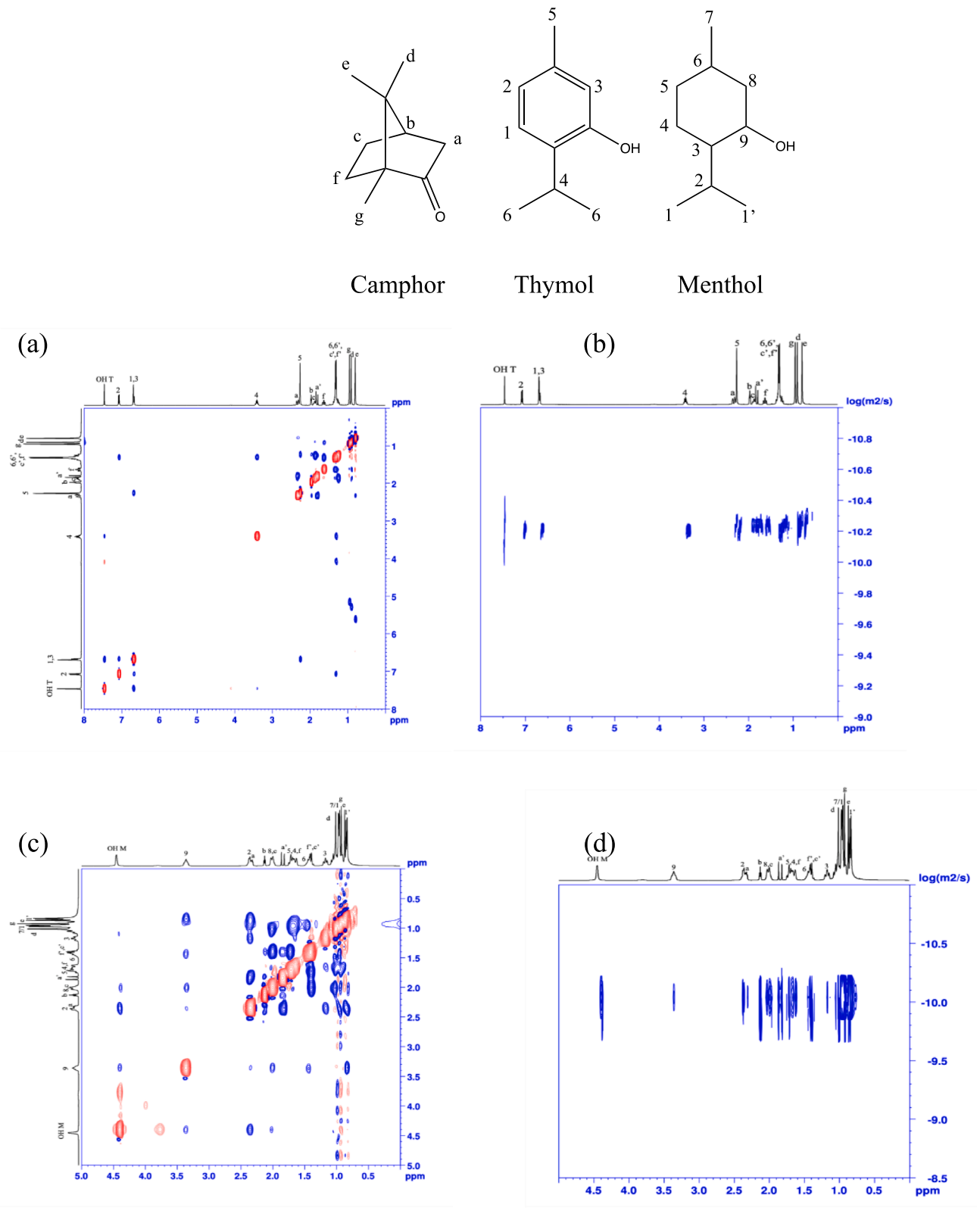

Fig. 1. Spectra of the binary studied mixtures. (a) NOESY and (b) DOSY of camphor:thymol (1:1); (c) NOESY and (d) DOSY of camphor:menthol (1:2).

can accept two hydrogen bonds from T, while T will only donate one hydrogen bond with C. Note that the aromatic π system of T influences its hydroxyl group, increasing its acidity, increasing its hydrogen bond donor behavior and therefore favoring the interaction with the carbonyl group of C. In dilution, the breaking interactions provoke both species to move independently showing similar values to each other according to the similarity of their molar masses. Again, C exhibited a lower value than T, so some interactions could remain at that dilution percentage. Also, the ratio D_T/D_C was close to those of the pure compounds (Table 3).

For the C:M (1:2) mixture, the spectra (Fig. S2) did not show decomposition reactions and, again confirmed that the stoichiometry of

Table 3
The diffusion coefficients (D) at 300 K of pure compounds diluted in $CDCl_3$ (30 mg • ml^{-1}), neat hESs, and diluted hESs with 90 % $CDCl_3$ of several species: aliphatic hydrogens of thymol or menthol (HBD), aliphatic hydrogens of camphor (C), aliphatic hydrogens of lidocaine (L), and hydroxyl hydrogen of thymol or menthol in binary mix or amine hydrogen of lidocaine in ternary mix (H–HBD).

System	$10^{10}D_C$/ $m^2{\cdot}s^{-1}$	$10^{10}D_{HBD}$/ $m^2{\cdot}s^{-1}$	$10^{10}D_L$/ $m^2{\cdot}s^{-1}$	$10^{10}D_{H-HBD}$/ $m^2{\cdot}s^{-1}$
Diluted camphor	18.08 ± 0.02	–	–	–
Diluted thymol	–	17.64 ± 0.03	–	17.69 ± 0.03
Diluted menthol	–	19.23 ± 0.04	–	19.29 ± 0.04
Diluted lidocaine	–	–	15.69 ± 0.03	15.79 ± 0.03
Camphor:thymol (1:1)	0.477 ± 0.001	0.509 ± 0.001	–	0.512 ± 0.005
Diluted camphor: thymol (1:1)	12.30 ± 0.01	12.41 ± 0.02	–	–
Camphor:menthol (1:2)	0.587 ± 0.001	0.507 ± 0.001	–	0.524 ± 0.005
Diluted camphor: menthol (1:2)	11.91 ± 0.05	12.09 ± 0.06	–	–
Camphor:thymol: lidocaine (1:1:1)	0.230 ± 0.003	0.175 ± 0.008	0.147 ± 0.002	0.196 ± 0.005
Diluted camphor: thymol:lidocaine (1:1:1)	10.77 ± 0.17	9.31 ± 0.17	7.74 ± 0.06	–
Camphor:menthol: lidocaine (1:2:1)	0.469 ± 0.020	0.408 ± 0.005	0.311 ± 0.008	0.394 ± 0.005
Diluted camphor:menthol: lidocaine (1:2:1)	12.09 ± 0.04	12.14 ± 0.08	9.175 ± 0.11	–

$D_{CDCl_3} = 28{\cdot}10^{-10}m^2{\cdot}s^{-1}$ [46]; D_{CDCl_3}=$26.50{\cdot}10^{-10}m^2{\cdot}s^{-1}$ this work obtained as the average of D values for each experiment for pure compounds.

the mixture is correct. A greater number of NOESY cross-peaks were detected (Fig. 1c) than in the previous mixture which is in agreement with the larger number of signals from M. It is worth mentioning that the overlapping observed between C and M protons difficults their analysis. Again, all the cross-peaks were positive and intracomponent, that is M−M and C–C, and no interactions between C and M were observed. Therefore, these signals can be in agreement with the presence of dispersive interactions within the same components however the formation of a strong supramolecular structure was not favoured. Fig. 1d displays the DOSY spectrum of the neat sample in which three traces are found. The D coefficients were similar to the previous mixture (Table 3) but present slight differences. Even though C:M (1:2) mixture presented a slightly higher value of viscosity at 300 K (Table S2), the D values of the neat mixture with M were higher than those of the hES with T. This fact suggests a higher presence of interactions between T and C as it has been shown by NMR experiments exposed above. Also, unlike C:T (1:1) mixture, C presented higher mobility than the terpene (M). This fact could be due to the M−M hydrophobic interactions that were detected in the NOESY experiments. The composition of the mixture and the capability of M to act as HBA or HBD favoured the interactions of the terpene with itself [45]. In this way, C tends to diffuse independently exhibiting higher D coefficient than in C:T (1:1) mixture. As expected, the values in the diluted mixture were much higher than in the neat sample and were similar for C and M.

3.2. Thermophysical study

To characterize the two studied mixtures, six thermophysical properties such as density (ρ), speed of sound (u), refraction index (n_D), isobaric molar heat capacity ($C_{p,m}$), surface tension (γ), and kinematic viscosity (ν) were measured. From the product of ν and ρ, the dynamic viscosity (η) was calculated and tabulated instead of ν. The operating pressure was 0.1 MPa and the temperature ranged from 278.15 to 338.15 K for all properties except for n_D. Due to operational problems, the lower temperature for n_D was 283.15 K. Table S1 and S2 (Supplementary File) collect the measured values at all temperatures and Table 4 lists the experimental and calculated properties at 298.15 K and those found in the literature.

The ρ, u, and n_D are three properties whose values in a mixture are related to both the structure of the different components and the type and strength of the interactions between them. The more effective the molecular packing, the higher the values of $\rho, u,$ and n_D. The molecular motion increases with temperature, which makes fluid packing difficult increasing the volume occupied by a mole of fluid. Thus, the relationship found between these properties and temperature is usually linear with negative slope. For our mixtures, the parameters are reported in Table 5 and the graphical representation is shown in Fig. 2.

The density is a basic physicochemical property in the solvents and one of the most determined. According to the Hole Theory, a liquid can be seen as a continuum crossed by holes. Its volumetric behaviour is determined by the size of holes and how they are modified when variables such as temperature change. The larger the holes, the lower the density [47]. Considering that the aromatic ring is a flatter structure than that of cyclohexane, it is expected that the mixture with T to be denser than that of M. In fact, the ρ of C:T (1:1) mixture was close to 55 $kg{\cdot}m^{-3}$ greater than that of C:M (1:2) (Tables 4 and S1, Fig. 2a). In mixtures with hydrophobic character as the ours, the comparison between their values and those of water under similar conditions is very important for applications such as liquid–liquid extractions in an aqueous medium. Both mixtures presented densities lower than that of water. At 298.15 K, the difference between the density of the water and that of the mixture with T was 3 % and respect to that with M was 8 %. Then, the latter would be more appropriate from an operational point of view.

In the literature, we only found density data of C:T (1:1) mixture for comparison. The mean relative deviation between our data and those published by Martins et al. [34] over all temperature range was$MRD(\rho)$ = 0.015 %. At 298 K, the value measured in this work also agreed with that reported by Abdallah et al. [33] (Table 4). Equations of state (EoS) are very useful tools to predict the thermodynamic behaviour of systems under conditions different from those determined experimentally. They are usually applied in the design of the industrial operations after validation for the systems of interest. In this work, we have verified the PC-SAFT EoS for the C:T or M systems. A summary of the model can be found in the supplementary file and the values of the parameters of the pure compounds needed to apply it are listed in Table S3. It should be noted that a predictive calculation was performed using a null binary interaction parameter (k_{ij} = 0). Thus, the model predicted well the density of both mixtures (Fig. S3a) with a mean relative deviation of 0.23 % for the mixture with T and 0.20 % for that with M. In industry, the behaviour of liquids in the faces of temperature changes is a factor to consider and can be evaluated from the isobaric expansibility,α_p :

$$\alpha_p = -\frac{1}{\rho}\left(\frac{\partial\rho}{\partial T}\right)_p \tag{3}$$

The α_p values at 298.15 K are listed in Table 4 and those at several temperatures are shown in Fig. 3a. The expansibility was up to 10 % higher in the mixture with M. The influence of temperature on this property was linear ($R^2 > 0.999$) and it was also greater for this mix. The temperature coefficients were $\left(\partial\alpha_p/\partial T\right) = 6.3{\cdot}10^{-4}$ and $7.1\ {\cdot}10^{-4}\ kK^{-2}$ for C:T (1:1) and C:M (1:2), respectively. An increase in temperature implies an increase in thermal energy, which generates fluctuations in the positions of the molecules, increasing the free space between them.

The values of the speed of sound were higher for the mixture with T

Table 4
Experimental and calculated properties[a] of camphor:thymol (1:1) and camphor:menthol (1:2) eutectic mixtures at $T = 298.15$ K and $p = 0.1$ MPa.

Experimental properties	Camphor:thymol(1:1)	Camphor:menthol(1:2)	Calculated properties	Camphor:thymol(1:1)	Camphor:menthol(1:2)
Density ρ/kg·m^{-3}	966.98/966.8[b]/ 967.50[c]	912.41	Isobaric expansibility α_p/kK^{-1}	0.786	0.833
Speed of sound u/m·s^{-1}	1410.46	1362.28	Isentropic compressibility κ_s/TPa^{-1}	519.83	590.58
Refraction index n_D	1.49654/1.4970[c]	1.46165	Free intermolecular length L_f/Å	0.451	0.480
Isobaric molar heat capacity $C_{p,m}$/J·mol^{-1}·K^{-1}	256	278	Molar refraction R_m/cm^3·mol^{-1}	45.75	46.64
Surface tension γ/mN·m^{-1}	32.30/30.35[c]	29.22	Entropy of surface ΔS_S/mN·m^{-1}·K^{-1}	0.0755	0.0637
Dynamic viscosity η/mPa·s	20.817/20.8[b]/ 21.10[c]	21.359	Enthalpy of surface ΔH_S/mN·m^{-1}	54.81	48.20
			Activation energy of viscous flow $E_{a,\eta}$/kJ·mol^{-1}	39.68	48.13

[a]Standard uncertainties are: $u(T)$=0.005 K for ρ and u, 0.5 K for $C_{p,m}$, and 0.01 K for the rest of properties. The combined expanded uncertainties (0.95 level of confidence, k=2) are $U_c(\rho) = 0.05$ kg·m^{-3}; $U_c(u)$=0.5 m·s^{-1}; $U_c(n_D)$=2·10^{-5}; $U_c(C_{p,m})$=1%; $U_c(\gamma) = 1$ %; $U_c(\eta)$=1%; $U_c(\alpha_p)$=0.04 kK^{-1}; $U_c(\kappa_s)$=0.22 TPa^{-1}; $U_c(L_f)$=0.005 Å; $U_c(R_m)$=0.004 cm^3·mol^{-1}; $U_c(f_m)$=0.03 cm^3·mol^{-1}; $U_c(\Delta S_S)$=0.001 mN·m^{-1}·K^{-1}; $U_c(\Delta H_S)$=0.06 mN·m^{-1}. [b]Ref. [34]; [c]Ref. [33].

Table 5
Fit parameters (A_Y, B_Y, C_Y) and the regression coefficients, R^2, for the thermophysical properties of camphor:thymol (1:1) and camphor:menthol (1:2) eutectic mixtures.

Mixture	Property	A_Y	B_Y	C_Y	R^2
Camphor:thymol (1:1)	Density ρ^a/kg·m^{-3}	1193.74	–0.7604		1
	Speed of sound u^a/m·s^{-1}	2459.92	–3.5189		0.9999
	Refraction index n_D^a	1.62336	–4.2·10^{-4}		0.9999
	Isobaric molar heat capacity $C_{p,m}^a$/J·mol^{-1}·K^{-1}	–164.73	1.414		0.9997
	Surface tension γ^a/mN·m^{-1}	54.938	–0.0762		0.9979
	Dynamic viscosity η^b/mPa·s	0.02923	804.46	175.72	0.9999
Camphor:menthol (1:2)	Density ρ^a/kg·m^{-3}	1138.90	–0.7599		0.9999
	Speed of sound u^a/m·s^{-1}	2391.51	–3.4493		0.9998
	Refraction index n_D^a	1.58561	–4.1·10^{-4}		0.9999
	Isobaric molar heat capacity $C_{p,m}^a$/J·mol^{-1}·K^{-1}	–242.65	1.744		0.9998
	Surface tension γ^a/mN·m^{-1}	48.701	–0.0654		0.9988
	Dynamic viscosity η^b/mPa·s	0.01869	763.05	189.90	0.9999

[a] $Y = A_Y + B_Y T$; [b] $Y = A_Y \exp\left(\frac{B_Y}{T - C_Y}\right)$; T in K.

(Tables 4 and S1, Fig. 2b). From u and ρ data at similar conditions, the compression capacity of the fluid at constant entropy (κ_S) was calculated and the free intermolecular length (L_f) was estimated using the Jacobson' constant (K). The equations are:

$$\kappa_S = \frac{1}{\rho u^2} \tag{4}$$

$$L_f = K\sqrt{\kappa_S} = (91.368 + 0.3565T) \bullet 10^{-8}\sqrt{\kappa_S} \tag{5}$$

Both properties will be greater in the less compact fluid and will increase with T as it occurs in the studied mixtures (Table 4 and Fig. 3b). The influence of temperature on κ_S was linear ($R^2 > 0.995$) for both mixtures with the coefficients: $(\partial\kappa_S/\partial T)$=3.285 TPa^{-1}·K^{-1} for C:T (1:1) and 3.805 TPa^{-1}·K^{-1} for C:M (1:2).

Similarly to above, the values of the refraction index of C:T (1:1) mixture were higher than those with M (Tables 4 and S1) and decreased with increasing T (Fig. 2c). For the first mixture, our value of n_D at 298.15 K was in agreement with that found in literature (Table 3). From n_D and ρ data at the same p and T, the molar refraction (R_m) is calculated with the Lorentz-Lorentz equation:

$$R_m = \left(\frac{n_D^2 - 1}{n_D^2 + 2}\right)\frac{M}{\rho} \tag{6}$$

where M is the molar mass of the mixture calculated as the sum of mole contributions of each component in the mixture: $M = \sum_i M_i x_i$. The R_m indicates the ability of a molecule to distort its charge distribution when an electric field is applied to it. It is related to the hard-core volume of a mole of molecules so the difference between the molar volume and the molar refraction is an estimation of the free volume or size of the holes (f_m). The R_m was higher for the mixture with M and the dependence on T

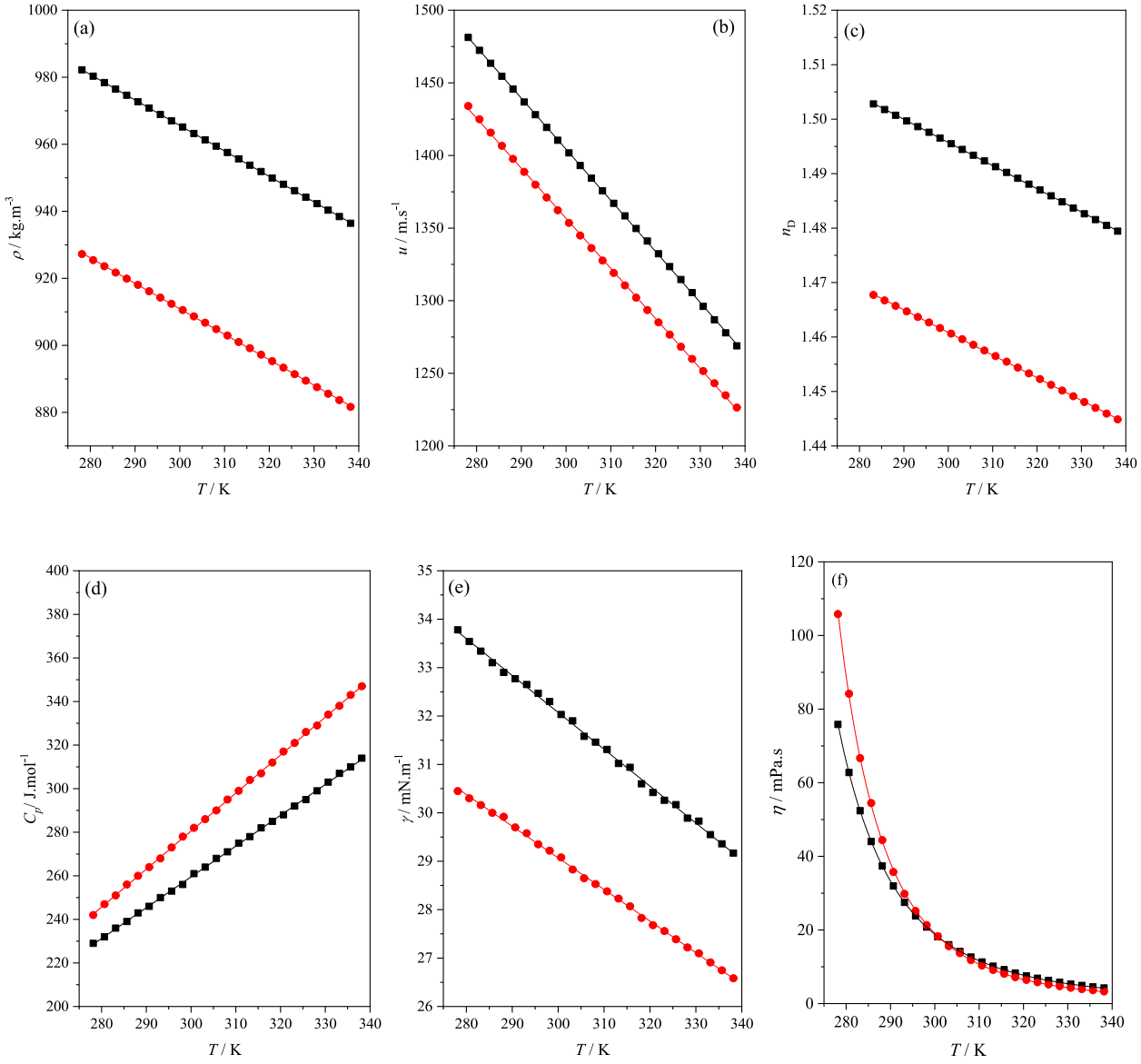

Fig. 2. Experimental thermophysical properties of camphor-based eutectic solvents at several temperatures and at $p = 0.1$ MPa. (a), density, ρ; (b) speed of sound, u; (c) refraction index, n_D; (d) isobaric molar heat capacity, $C_{p,m}$; (e) surface tension, γ; (f) dynamic viscosity, η. (■), Camphor:thymol (1:1); (●), Camphor:menthol (1:2). Points, experimental values; lines, correlated data.

was small in both cases (Table 4, Fig. 3c). Moreover, the f_m of the C:M (1:2) was up to 2.8 % higher than C:T (1:1) with a temperature dependence more pronounced than that R_m (Fig. 3d). Considering the molar and the free volumes at 298.15 K, the percentages of unoccupied volume in C:T (1:1) and C:M (1:2) mixtures were 70.7 % and 72.7 %, respectively.

The isobaric molar heat capacity ($C_{p,m}$) indicates the energy needed to increase the temperature of a mole of a substance by one degree. In pharmacology, it is an important property to establish drug processing and storage conditions. The values measured were higher for the C:M (1:2) mixture and the difference increased with T increasing (Fig. 2d). In the literature, several simple correlations to estimate the isobaric heat capacity of the ESs have been proposed [48]. Among them, we have chosen the one published by Taherdazeh et al. [49] because is the newest and the one with the best results. To apply it, the values of the molar mass, the critical properties, and the acentric factor of the mixture are needed. The equations are reported in the supplementary file. In our mixtures, the model overestimated the $C_{p,m}$ values with a deviation for the mixtures with T and M of 11 % and 7.7 %, respectively. Thermodynamic models such as PC-SAFT EoS are useful tools to estimate this property although the deviation of the experimental value is commonly higher than in the modeling of the density. The mean relative deviations calculated in the $C_{p,m}$ prediction of the C:T (1:1) and C:M (1:2) mixtures were 6.8 % and 5.5 %, respectively. Fig. S3b shows the graphical comparison.

The surface tension of a liquid is related to the energy consumed by expanding the air-liquid interface and therefore, with the interactions within the fluid. The weakening of the cohesive forces by the increase of the temperature diminishes the differences in the structure of the liquids. So, the more structured the liquid, the higher the surface tension. Also, the differences of γ of several fluids are less at higher temperatures. The γ of C:T (1:1) was higher than that of C:M (1:2) (Tables 4 and S1) which can be due to the presence of the aromatic ring that, unlike the cyclic, can establish π-π interactions with the neighbors similar molecules that hinder the expansion of the interface. The differences of γ between both systems decreased with increasing the temperature (Fig. 2e). They were 3.3 mN·m^{-1} at 278.15 K and 2.59 mN·m^{-1} at 338.15 K. At the critical temperature (T_c), the surface tension of fluids

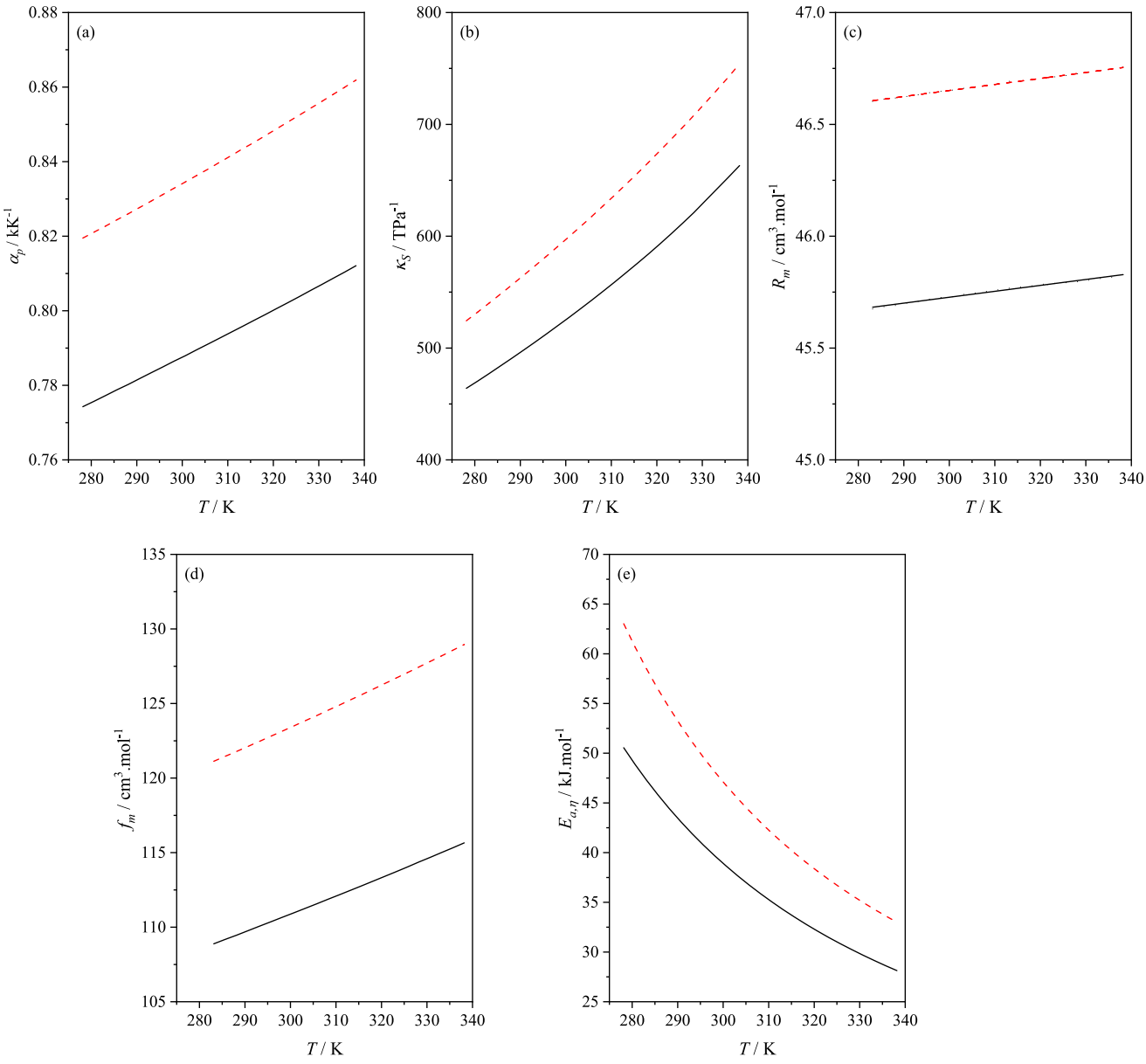

Fig. 3. Calculated properties of camphor-based eutectic solvents at several temperatures and at p = 0.1 MPa. (a) Isobaric expansibility, α_p, (b) isentropic compressibility, κ_s; (c) molar refraction, R_m; (d) free volume, f_m; (e) energy of the viscous flow, $E_{a,\eta}$. (▬), Camphor:thymol (1:1); (▬ ▬), Camphor:menthol (1:2).

became null so the γ measured at several T can be used to estimate this interesting property in the modeling of fluids but difficult to determine. The values calculated from Guggenheim and Eötvos equations [50,51] are listed in Table S4. In addition, we have used PC-SAFT EoS to calculate the T_c and critical pressure (p_c) of both studied systems. T_c and p_c data are reported in Table S4 and displayed in Fig. S4. From γ and the γ–T relationship, the entropy of surface (ΔS_S) and the enthalpy of surface (ΔH_S) were calculated with the equations:

$$\Delta S_S = -\left(\frac{\partial \gamma}{\partial T}\right)_p \tag{7}$$

$$\Delta H_S = \gamma - T\left(\frac{\partial \gamma}{\partial T}\right)_p \tag{8}$$

Table 4 lists the values of both thermodynamic properties at 298.15 K and as expected, they were higher in the mixture with T.

The viscosity of a fluid indicates the opposition exerted by the molecules to its tangential displacement. In solubility processes, viscosity greatly influences the rate of dissolution. The higher the viscosity, the slower the dissolution rate. Almost all the values determined in this work (Tables 4 and S1) were less than 100 mPa • s, the value that is considered the maximum viscosity for proper industrial operation. The influence of temperature on transport properties is more pronounced at low temperatures, so the η–T correlation is usually exponential. Table 5 lists the fitting parameters (A, B, C) of the exponential VFT equation. From them, the activation energy of viscous flow ($E_{a,\eta}$) defined as the energy required to overcome the frictional forces of neighboring molecules can be calculated:

$$E_{a,\eta} = R\left(\frac{\partial \ln \eta}{\partial\left(\frac{1}{T}\right)}\right) = R\frac{B}{\left(\frac{C^2}{T^2} - \frac{2C}{T} + 1\right)} \tag{9}$$

The viscosity of a fluid depends on both intermolecular interactions and the shape of the molecules. At temperatures below 302 K, the C:M (1:2) mixture had a higher η and a lower $E_{a,\eta}$ than that of the aromatic terpene (Table 4, Fig. 2f,3e). It seems that although T was able to

establish more interactions generating a more compact mixture, at low temperatures the structure of the M cycle hindered the molecular motion between neighboring layers. For the C:T (1:1) mixture, we compared our data with those from the literature. The mean relative deviation with data from Martins et al. [34] in the studied T range was$MRD(\eta) = 0.38$ % and the deviation with the value from Abdallah et al. [33] at 298 K was less than 0.3 mPa·s (Table 4). No η data of C:M (1:2) was found.

Surface tension is related to the probability of finding a hole with a radius greater than the molecular radius [47]. The higher its value, the lower this probability and, consequently, the lower the ability of the

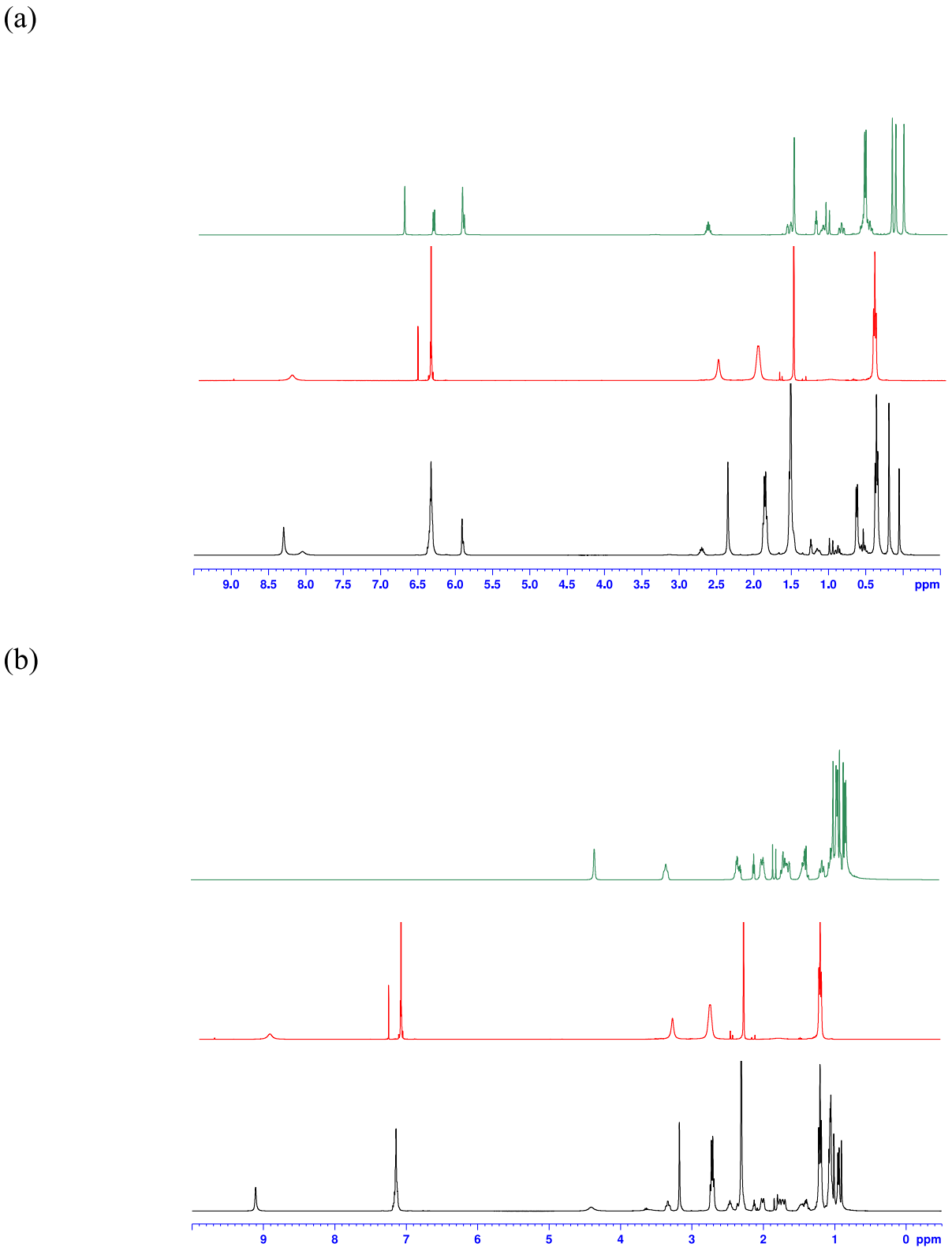

Fig. 4. Comparative of ^{1}H −NMR spectra. From top to bottom: eutectic binary mixture, pure lidocaine, and ternary mixture. (a) Camphor:thymol:lidocaine (1:1:1); (b) Camphor:menthol:lidocaine (1:2:1).

fluid to generate holes where the molecules can pass through each other. Therefore, correlations between surface tension and viscosity can be found. The equations proposed by Pelofsky and Mukherjee [52] are found in the supplementary file and the parameters fitted from our data are collected in Table S5. The regression coefficients ($R^2 > 0.95$) allowed us to validate the experimental data.

The results from ρ, u, n_D, γ and η data above presented, in which the systems with T showed more effective compactions and fluidity than those with M, coincided with the results in other systems previously obtained by us [39,40,53].

3.3. Solubility study

The solubility of L in water measured in this work was $W_L = 3.62$ mg_L/g_S and it matched with that found in the literature [54]. On the other hand, L was extremely soluble in the eutectic mixtures with values of $W_L = 1954.47$ mg_L/g_S ($x_L = 0.55$, in mole fraction) and 1523.45 mg_L/g_S ($x_L = 0.48$) for C:T (1:1) and C:M (1:2), respectively. Li et al. [54] measured the solubility of this API in two deep eutectic solvents whose composition was choline chloride:glycolic acid (1:2) and choline chloride:glycolic acid:oxalic acid (1:1.7:0.3). The values were 0.1 and 0.3 g_L/g_S, respectively. As expected, they were lower than ours due to those mixtures having hydrophilic nature. To understand the marked increase in the solubility (up to 540-fold), we have carried out a spectroscopic study of the ternary mixtures C:T:L (1:1:1) and C:M:L (1:2:1). The compositions were chosen to avoid the potential precipitation of L in the apparatus from the saturated solutions.

Figures S5 and S6 show the ^{1}H NMR and ^{13}C NMR spectra of both ternary mixtures. A comparison of the ^{1}H NMR spectra of the binary mixture, pure L in $CDCl_3$, and the ternary mixture of each system can be found in Fig. 4a and 4b. The spectra almost overlapped with slight changes in the chemical environment and with no reaction or decomposition of L being detected. An increase of 1 ppm in the chemical shift of the OH of T concerning the binary mixture was observed, probably, due to the establishment of hydrogen bonds with lidocaine. L acts as HBA retracting electron density from the proton donated by T. This unshielding would confirm its ability and preference to act as a hydrogen bond donor [55]. Also, it is worth noting the increase in resolution in the ternary mixture for the signals of lidocaine, especially those corresponding to the three methylene groups next to the aminic nitrogen atom (F and G protons). The presence of broad signals can be due to medium-slow conformational equilibria due to the pyramidalization isomerization of the nitrogen atom. Therefore, the increase of resolution can indicate either a faster interconversion equilibrium (which is the more probable scenario) or a total cessation of the pyramidalization process, due to both effects to the strong interaction of the nitrogen atom with the environment. This is in agreement with that explained above and it suggests the formation of a supramolecular structure, a DES distinctive feature.

For the C:T:L equimolar ternary mixture, several intra and intermolecular cross-peaks (nOe contacts) were detected for all components from the NOESY spectrum (Fig. 5a). L and T presented a large number of negative cross-peaks (same sign as diagonal) corresponding to intra- and intermolecular interactions between both compounds as well as of exchange of the mobile hydrogens (NH and OH protons). These interactions were of different types, including dispersive and van der Waals interactions and probably hydrogen bonds between the amine group of L and the hydroxyl group of T. In the first group, we can include interactions between aromatics protons of T (1,2 and 3 protons) and L (A, B, and C protons) and between methyl groups of T (5 and 6 protons) and L (D, E and H protons). As previously reported, the presence of negative cross-peaks has been associated with the formation of a strong supramolecular structure. Interestingly, positive intramolecular and negative intermolecular signals were observed for camphor. Of the latter, the most intense were due to the proximity of the methyl groups of C (e,d and g protons) with aromatic (A, B and C protons) and aliphatic protons of L (H, G, F, D and E protons). The intensity of signals between methyl groups of C and T, both aromatic and aliphatic protons, was slightly lower. Negative cross-peaks correlating aliphatic protons in C (a, b,c, and f protons) and protons of L appeared with lower intensity, probably due to the amount of protons (compared to methyl groups), and with even lower intensity, those correlating with protons of T. Positive signals of C are due to intramolecular contacts. The differences in camphor signals could be explained by considering that a stronger supramolecular structure was established between L and T and that C was dissolved in it with reduced interactions with the other two components. In this way, positive signals of C can be related to C molecules which are not part of the supramolecular structure, while negative NOEs point out how C molecules interact with the network established between L and T molecules. Probably, this situation is very dynamic and, C molecules constantly become part and leave the supramolecular network.

Diffusion coefficients (D) of the species in both the neat and diluted (90 % $CDCl_3$) ternary mixture and the results are listed in Table 3. For the neat, the experiments showed 4 traces (Fig. 5b) corresponding to the aliphatic and aromatics hydrogens of each component and the mobile hydrogen of the L, the mobile hydrogen of T was not detected in this experiment. The D values of C were higher than for the other components. Moreover, thymol diffused more slowly than camphor in the ternary mixture unlike in the binary one. All of this would show the formation of an LT supramolecular structure and the dissolution of C in LT. For the diluted, only the non-mobile aliphatic signals were detected and the mobility was increased considerably. Considering the parallel molar mass of T and C (Table 1), a similar diffusivity of both free components in the same solvent could be expected. Nevertheless, T presented an intermediate value between C and L, so some T–L interaction seems to persist despite the dilution. The lower value of L would be related to its greater mass.

For the C:M:L mixture, the NOESY spectrum (Fig. 5c) again exhibited both negative and positive cross-peaks. The observed number of signals was lower compared to the C:T:L mixture, suggesting the formation of a strong supramolecular structure is less favored in this system. The majority of negative cross-peaks were observed among protons from L, both intramolecular and the other mixture components. Only the cross-peak between protons H and G in lidocaine appeared with a positive sign, probably due to the strong scalar coupling between them. The most intense negative signals correspond to L-L interactions via methyl groups (D, E, and H protons) and L-M interactions involving methyl groups of M (1 and 7 protons) and L (D/E protons), as well as between methyl groups of M and aromatics protons of L (A, B and C protons). The chemical exchange of mobile protons between M and L was also detected. On the other hand, C presented positive intramolecular signals, and no peaks with the other components were observed, in contrast to the previous system. These results suggest the formation of a weaker supramolecular network between M and L, compared to the previous system containing thymol, with C playing a more secondary role in this mixture, possibly due to the weaker hydrogen bonds formed between M and C compared to T. The values for the diffusion coefficient in the neat C:M:L mixture (Table 3) were similar for the three aliphatic species detected in DOSY experiments. Based on viscosity data of eutectic mixtures composed of thymol and menthol previously reported by our group [40,53], it would be expected that the mixture with menthol would present lower D values than the C:T:L mixture. However, similar to what occurred when comparing C:T (1:1) and C:M (1:2) mixtures, it was observed that C:M:L (1:2:1) mixture practically doubles the C:T:L (1:1:1) diffusion values. This highlights that the diffusion of the components in these ternary mixtures is dominated by the lidocaine content and the interactions established between the terpene and lidocaine. This also suggests that thymol, probably because of its HBD capacity and the presence of its aromatic ring, tends to form stronger interactions with lidocaine than menthol, which is also reflected in the diffusion characteristics of the mixtures.

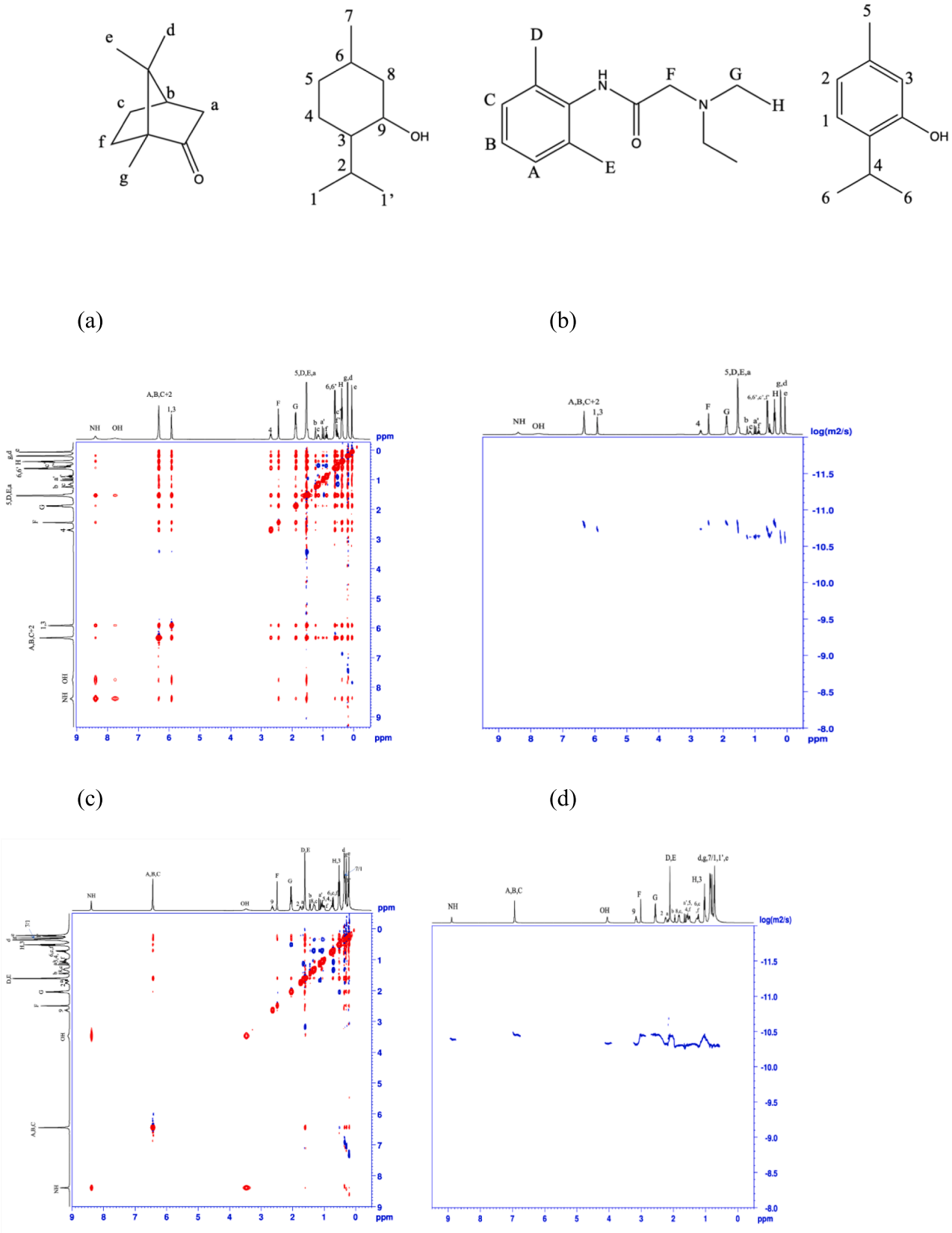

Fig. 5. Spectra of the ternary studied mixtures. (a) NOESY and (b) DOSY of camphor:thymol:lidocaine (1:1:1); (c) NOESY and (d) DOSY of camphor:menthol: lidocaine (1:2:1).

In summary, the above results indicated that L had a great tendency to form eutectic solvents, interacting strongly with T and M, especially with T, and weakly with C such as literature reports for the corresponding binary eutectics [56–58]. The cross-peaks detected between M and L or C were fewer and less intense than in the system containing T, which would highlight the importance of the aromatic ring in the structure of the eutectic system, both increasing the HBD character of T and allowing the establishment of aromatic interactions. Considering the most intense cross-peaks observed, the nature of the detected intermolecular interactions in the ternary mixtures were both the hydrogen bonds and the hydrophobic interactions involving highly nonpolar methyl groups and aromatic rings.

4. Conclusions

Two hydrophobic eutectic solvents (hESs) composed of camphor and thymol or menthol were studied in this work. The structural characterization was performed with one and two-dimensional NMR techniques. From them, the diffusion coefficients of the species presented in the mixtures were calculated. In addition, several thermophysical properties were measured and discussed. They were the density, the speed of sound, the refraction index, the isobaric molar heat capacity, the surface tension, and the viscosity. Finally, the solubility of lidocaine in water and in these hESs was determined with the shake-flask method and evaluated by NMR spectroscopy.

The NMR spectra of both hESs showed the majority presence of hydrophobic interactions between components and the absence of a hydrogen bond network. The thermophysical study showed that the equimolar C:T mixture had more effective compaction and greater fluidity than the C:M (1:2) mixture. The solubility of L strongly increased in these hESs compared to that determined in water. The ratio $W_L(\text{hESs})/W_L(H_2O) = 540$ for C:T(1:1) and 420 for C:M (1:2). The spectroscopic results showed the following sequence in the interactions between L and the rest of the components: T > M > C.

CRediT authorship contribution statement

Nuria Padilla: Resources, Methodology, Data curation. **Ignacio Delso:** Methodology, Formal analysis. **Fernando Bergua:** Writing – original draft, Formal analysis. **Carlos Lafuente:** Writing – original draft, Validation. **Manuela Artal:** Writing – review & editing, Writing – original draft, Supervision.

Declaration of competing interest

The authors declare that they have no known competing financial interests or personal relationships that could have appeared to influence the work reported in this paper.

Data availability

All data generated or analyzed during this study are included in this published article and its Supplementary Information files.

Acknowledgments

PLATON research group acknowledges financial support from Gobierno de Aragón and Fondo Social Europeo “Construyendo Europa desde Aragón” E31_23R.

Appendix A. Supplementary data

Supplementary data to this article can be found online at https://doi.org/10.1016/j.molliq.2024.125069.

References

[1] S.N. Pedro, M.G. Freire, C.S.R. Freire, A.J.D. Silvestre, Deep eutectic solvents comprising active pharmaceutical ingredients in the development of drug delivery systems, Expert Opin. Drug Deliv. 16 (2019) 497–506, https://doi.org/10.1080/17425247.2019.1604680.
[2] C.W. Pouton, Formulation of poorly water-soluble drugs for oral administration: Physicochemical and physiological issues and the lipid formulation classification system, Eur. J. Pharm. Sci. 29 (2006) 278–287, https://doi.org/10.1016/j.ejps.2006.04.016.
[3] A. Singh, Z.A. Worku, G. Van den Mooter, Oral formulation strategies to improve solubility of poorly water-soluble drugs, Expert Opin. Drug Deliv. 8 (2011) 1361–1378, https://doi.org/10.1517/17425247.2011.606808.
[4] S. Emami, A. Shayanfar, Deep eutectic solvents for pharmaceutical formulation and drug delivery applications, Pharm. Dev. Technol. 25 (2020) 779–796, https://doi.org/10.1080/10837450.2020.1735414.
[5] S.N. Pedro, C.S.R. Freire, A.J.D. Silvestre, M.G. Freire, Deep Eutectic Solvents and Pharmaceuticals, Encyclopedia 1 (2021) 942–963, https://doi.org/10.3390/encyclopedia1030072.
[6] M.H. Zainal-Abidin, M. Hayyan, G.C. Ngoh, W.F. Wong, C.Y. Looi, Emerging frontiers of deep eutectic solvents in drug discovery and drug delivery systems, J. Control. Release 316 (2019) 168–195, https://doi.org/10.1016/j.jconrel.2019.09.019.
[7] W. Lu, H. Chen, Application of deep eutectic solvents (DESs) as trace level drug extractants and drug solubility enhancers: State-of-the-art, prospects and challenges, J. Mol. Liq. 349 (2022) 118105, https://doi.org/10.1016/j.molliq.2021.118105.
[8] M.Q. Farooq, N.M. Abbasi, E.A. Smith, J.W. Petrich, J.L. Anderson, characterizing the solvation characteristics of deep eutectic solvents composed of active pharmaceutical ingredients as a hydrogen bond donor and/or acceptor, ACS Sustain. Chem. Eng. 10 (2022) 3066–3078, https://doi.org/10.1021/acssuschemeng.1c08675.
[9] A.R.C. Duarte, A.S.D. Ferreira, S. Barreiros, E. Cabrita, R.L. Reis, A. Paiva, A comparison between pure active pharmaceutical ingredients and therapeutic deep eutectic solvents: Solubility and permeability studies, Eur. J. Pharm. Biopharm. 114 (2017) 296–304, https://doi.org/10.1016/j.ejpb.2017.02.003.
[10] M.A.R. Martins, S.P. Pinho, J.A.P. Coutinho, Insights into the nature of eutectic and deep eutectic mixtures, J. Solution Chem. (2018), https://doi.org/10.1007/s10953-018-0793-1.
[11] E.L. Smith, A.P. Abbott, K.S. Ryder, Deep eutectic solvents (DESs) and their applications, Chem. Rev. 114 (2014) 11060–11082, https://doi.org/10.1021/cr300162p.
[12] D.J.G.P. Van Osch, L.F. Zubeir, A. Van Den Bruinhorst, M.A.A. Rocha, M.C. Kroon, Hydrophobic deep eutectic solvents as water-immiscible extractants, Green Chem. 17 (2015) 4518–4521, https://doi.org/10.1039/c5gc01451d.
[13] D.O. Abranches, J.A.P. Coutinho, Type V deep eutectic solvents: Design and applications, Curr Opin Green Sustain Chem 35 (2022) 100612, https://doi.org/10.1016/j.cogsc.2022.100612.
[14] D.O. Abranches, M.A.R. Martins, L.P. Silva, N. Schaeffer, S.P. Pinho, J.A. P. Coutinho, Phenolic hydrogen bond donors in the formation of non-ionic deep eutectic solvents: The quest for type v des, Chem. Commun. 55 (2019) 10253–10256, https://doi.org/10.1039/c9cc04846d.
[15] M. Zielińska-Błajet, P. Pietrusiak, J. Feder-Kubis, Selected monocyclic monoterpenes and their derivatives as effective anticancer therapeutic agents, Int. J. Mol. Sci. 22 (2021) 4763, https://doi.org/10.3390/ijms22094763.
[16] F. Xie, J. Chai, Q. Hu, Y. Yu, L. Ma, L. Liu, X. Zhang, B. Li, D. Zhang, Transdermal permeation of drugs with differing lipophilicity: Effect of penetration enhancer camphor, Int. J. Pharm. 507 (2016) 90–101, https://doi.org/10.1016/j.ijpharm.2016.05.004.
[17] T. Kotaka, S. Kimura, M. Kashiwayanagi, J. Iwamoto, Camphor induces cold and warm sensations with increases in skin and muscle blood flow in human, Biol. Pharm. Bull. 37 (2014) 1913–1918, https://doi.org/10.1248/bpb.b14-00442.
[18] C.D. Santos, J.C. Cabot, Persistent effects after camphor ingestion: A case report and literature review, J. Emerg. Med. 48 (2015) 298–304, https://doi.org/10.1016/j.jemermed.2014.05.015.
[19] K.A. Wojtunik-Kulesza, Toxicity of selected monoterpenes and essential oils rich in these compounds, Molecules 27 (2022) 1716, https://doi.org/10.3390/molecules27051716.
[20] FDA, Food-additives-petitions/food-additive-status-list, Www.Federalregister.Gov/d/2022-19294 (2022) 24–25.
[21] A. Escobar, M. Pérez, G. Romanelli, G. Blustein, Thymol bioactivity: A review focusing on practical applications, Arab. J. Chem. 13 (2020) 9243–9269, https://doi.org/10.1016/j.arabjc.2020.11.009.
[22] G.P.P. Kamatou, I. Vermaak, A.M. Viljoen, B.M. Lawrence, Menthol: A simple monoterpene with remarkable biological properties, Phytochemistry 96 (2013) 15–25, https://doi.org/10.1016/j.phytochem.2013.08.005.
[23] D.M. Bautista, J. Siemens, J.M. Glazer, P.R. Tsuruda, A.I. Basbaum, C.L. Stucky, S.-E. Jordt, D. Julius, The menthol receptor TRPM8 is the principal detector of environmental cold, Nature 448 (2007) 204–208, https://doi.org/10.1038/nature05910.
[24] F. Trebitsch, Antimicrobial action of thymol-camphor compared with 20 pharmaceutical preparations 1. Staphylococcus aureus, Aust. Dent. J. 23 (1978) 152–155, https://doi.org/10.1111/j.1834-7819.1978.tb02902.x.
[25] T. Raja Sekharan, R. Margret Chandira, S.C. Rajesh, S. Tamilvanan, C. T. Vijayakumar, B.S. Venkateswarlu, Ph, viscosity of hydrophobic based natural deep eutectic solvents and the effect of curcumin solubility in it, Biointerface Res.

Appl. Chem. 11 (2021) 14620–14633, https://doi.org/10.33263/BRIAC116.1462014633.
[26] M. Gohel, S. Nagori, Resolving issues of content uniformity and low permeability using eutectic blend of camphor and menthol, Indian J. Pharm. Sci. 71 (2009) 622, https://doi.org/10.4103/0250-474X.59543.
[27] C. Liu, J. Hu, H. Sui, Q. Zhao, X. Zhang, W. Wang, Enhanced skin permeation of glabridin using eutectic mixture-based nanoemulsion, Drug Deliv. Transl. Res. 7 (2017) 325–332, https://doi.org/10.1007/s13346-017-0359-6.
[28] M.C. Gohel, S.A. Nagori, Fabrication and design of transdermal fluconazole spray, Pharm. Dev. Technol. 14 (2009) 208–215, https://doi.org/10.1080/10837450802498936.
[29] S. Tuntarawongsa, T. Phaechamud, Polymeric eutectic system, Adv. Mat. Res. 528 (2012) 180–183, https://doi.org/10.4028/www.scientific.net/AMR.528.180.
[30] E. Santigosa, S. Pedersen-Bjergaard, M. Muñoz, M. Ramos-Payán, Green microfluidic liquid-phase microextraction of polar and non-polar acids from urine, Anal. Bioanal. Chem. 413 (2021) 3717–3723, https://doi.org/10.1007/s00216-021-03320-9.
[31] M. Paradkar, V. Thakkar, T. Soni, T. Gandhi, M. Gohel, Formulation and evaluation of clotrimazole transdermal spray, Drug Dev. Ind. Pharm. 41 (2015) 1718–1725, https://doi.org/10.3109/03639045.2014.1002408.
[32] M. Desai, A.M. Godbole, S. Somnache, P. Gajare, A. Pednekar, S. Manerikar, K. Kudaskar, V. Naik, Design, development, and characterization of film forming spray as novel antifungal topical formulation for superficial fungal infections, Indian J. Pharm, Educat. Res. 56 (2022) s651–s658, https://doi.org/10.5530/ijper.56.4s.211.
[33] M.M. Abdallah, S. Müller, A.G. de Castilla, P. Gurikov, A.A. Matias, M. do R. Bronze, N. Fernández, Physicochemical characterization and simulation of the eutectic solvent systems, Molecules 26 (2021) 1801–1816.
[34] M.A.R. Martins, L.P. Silva, N. Schaeffer, D.O. Abranches, G.J. Maximo, S.P. Pinho, J.A.P. Coutinho, Greener terpene-terpene eutectic mixtures as hydrophobic solvents, ACS Sustain. Chem. Eng. 7 (2019) 17414–17423, https://doi.org/10.1021/acssuschemeng.9b04614.
[35] P. Makoś, A. Przyjazny, G. Boczkaj, Hydrophobic deep eutectic solvents as “green” extraction media for polycyclic aromatic hydrocarbons in aqueous samples, J. Chromatogr. A 1570 (2018) 28–37, https://doi.org/10.1016/j.chroma.2018.07.070.
[36] R. Solaimalai, G. Shinde, A. Dharamsi, C. Kokare, Exploring the novel green eutectic solvent for the synthesis of 4-hydroxy-2-methyl- *N* -2-pyridinyl-2 *H* -1,2,-benzothiazine-3-carboxamide 1,1-dioxide with benzoic acid cocrystal using a co-grinding technique, New J. Chem. 44 (2020) 17088–17098, https://doi.org/10.1039/D0NJ03570J.
[37] X. Yang, X. Wei, Y. Mu, Q. Li, J. Liu, A review of the mechanism of the central analgesic effect of lidocaine, Medicine 99 (2020) e19898.
[38] P.J. Linstrom, W.G. Mallard, NIST Chemistry Webbok, NIST Standard Reference Database Number 69, Gaithersburg MD, 20899, 2020. DOI: 10.18434/T4D303.
[39] F. Bergua, M. Castro, J. Muñoz-Embid, C. Lafuente, M. Artal, Hydrophobic eutectic solvents: Thermophysical study and application in removal of pharmaceutical products from water, Chem. Eng. J. 411 (2021), https://doi.org/10.1016/j.cej.2021.128472.
[40] F. Bergua, M. Castro, J. Muñoz-Embid, C. Lafuente, M. Artal, L-menthol-based eutectic solvents: Characterization and application in the removal of drugs from water, J. Mol. Liq. 352 (2022) 118754, https://doi.org/10.1016/j.molliq.2022.118754.
[41] N. López, I. Delso, D. Matute, C. Lafuente, M. Artal, Characterization of xylitol or citric acid:choline chloride:water mixtures: Structure, thermophysical properties, and quercetin solubility, Food Chem. 306 (2020), https://doi.org/10.1016/j.foodchem.2019.125610.
[42] V. Antón, H. Artigas, J. Muñoz-Embid, M. Artal, C. Lafuente, Thermophysical study of 2-acetylthiophene: Experimental and modelled results, Fluid Phase Equilib. 433 (2017) 126–134, https://doi.org/10.1016/j.fluid.2016.10.026.
[43] E. Baka, Development and Examination Of Solubility Measurement Methods For Drug Solubility Determination, Smmelweis University, Budapest, 2010.
[44] I. Delso, C. Lafuente, J. Muñoz-Embid, M. Artal, NMR study of choline chloride-based deep eutectic solvents, J. Mol. Liq. 290 (2019) 111236, https://doi.org/10.1016/j.molliq.2019.111236.
[45] F. Bergua, Hydrophobic eutectic solvents: Characterization and application, Universidad de, Zaragoza (2022).
[46] D.L. Gurina, V.A. Golubev, Self-diffusion and molecular association in the binary systems dimethyl sulfoxide – chloroform and acetone – chloroform, Results Chem. 4 (2022) 100673, https://doi.org/10.1016/j.rechem.2022.100673.
[47] A.P. Abbott, R.C. Harris, K.S. Ryder, Application of hole theory to define ionic liquids by their transport properties, J. Phys. Chem. B 111 (2007) 4910–4913, https://doi.org/10.1021/jp0671998.
[48] A. Bagherzadeh, N. Shahini, D. Saber, P. Yousefi, S.M. Seyed Alizadeh, S. Ahmadi, F. Tat Shahdost, Developing a global approach for determining the molar heat capacity of deep eutectic solvents, Measurement 188 (2022) 110630, https://doi.org/10.1016/j.measurement.2021.110630.
[49] M. Taherzadeh, R. Haghbakhsh, A.R.C. Duarte, S. Raeissi, Estimation of the heat capacities of deep eutectic solvents, J. Mol. Liq. 307 (2020) 112940, https://doi.org/10.1016/j.molliq.2020.112940.
[50] E.A. Guggenheim, The principle of corresponding states, J. Phys. Chem. 13 (1945) 253–261.
[51] J.L.L. Shereshefsky, Surface tension of saturated vapors and the equation of Eötvos, J. Phys. Chem. 35 (1930) 1712–1720, https://doi.org/10.1021/j150324a014.
[52] A.H. Pelofsky, Surface tension-viscosity relation for liquids, J. Chem. Eng. Data 11 (1966) 394–397, https://doi.org/10.1021/je60030a031.
[53] F. Bergua, M. Castro, C. Lafuente, M. Artal, Thymol+l-menthol eutectic mixtures: Thermophysical properties and possible applications as decontaminants, J. Mol. Liq. 368 (2022) 120789, https://doi.org/10.1016/j.molliq.2022.120789.
[54] Z. Li, P.I. Lee, Investigation on drug solubility enhancement using deep eutectic solvents and their derivatives, Int. J. Pharm. 505 (2016) 283–288, https://doi.org/10.1016/j.ijpharm.2016.04.018.
[55] N. Schaeffer, D.O. Abranches, L.P. Silva, M.A.R. Martins, P.J. Carvalho, O. Russina, A. Triolo, L. Paccou, Y. Guinet, A. Hedoux, J.A.P. Coutinho, Non-Ideality in Thymol + Menthol Type v Deep Eutectic Solvents, ACS Sustain. Chem. Eng. 9 (2021) 2203–2211, https://doi.org/10.1021/acssuschemeng.0c07874.
[56] J.M. Edgecomb, E.E. Tereshatov, G. Zante, M. Boltoeva, C.M. Folden, Hydrophobic amine-based binary mixtures of active pharmaceutical and food grade ingredients: Characterization and application in indium extraction from aqueous hydrochloric acid media, Green Chem. 22 (2020) 7047–7058, https://doi.org/10.1039/d0gc02452j.
[57] R. Liu, J. Hao, Y. Wang, Y. Meng, Y. Yang, A separation strategy of Au(III), Pd(II) and Pt(IV) based on hydrophobic deep eutectic solvent from hydrochloric acid media, J. Mol. Liq. 365 (2022) 120200, https://doi.org/10.1016/j.molliq.2022.120200.
[58] U. Gala, M.C. Chuong, R. Varanasi, H. Chauhan, Characterization and comparison of lidocaine-tetracaine and lidocaine-camphor eutectic mixtures based on their crystallization and hydrogen-bonding abilities, AAPS PharmSciTech 16 (2015) 528–536, https://doi.org/10.1208/s12249-014-0242-4.